University of Crete
Faculty of Mathematics & Applied Mathematics

BACHELOR THESIS

Theoretical modeling of the interaction of ultrashort laser pulses with metals

Foundation for Research and Technology
Institute of Electronic Structure and Laser

FORTH
INSTITUTE OF ELECTRONIC STRUCTURE AND LASER

Antonios Stylianos Valavanis

Supervisor: Dr. Emmanuel Stratakis

Heraklion, November 2019

Abstract

The interaction of laser pulses with an array of solids (such as metals, semiconductors, dielectrics, polymers) have the ability to cause significant modifications in their surface and consequentially lead to remarkable changes in their optical and mechanical properties. A particularly distinct category of laser-matter interaction which allows the investigation of the existing mechanisms in short time scales, is highly recommended in the application of ultrashort laser pulses(in the femptoseconds (fs) time scale). The materials interaction with this kind of pulsing lasers, cause numerous of reliant operations in the spacetime interval which determine by the characteristics of the irradiation. In this thesis, a system of parabolic differential equations using computational techniques that were based on the finite difference method is presented for the purpose of understand the physical mechanisms that describe the response of the material after the irradiation. This technique will allow the investigation of thermal phenomena which occur both in the electron subsystem and in the lattice of the material. Ultimately, this will constitute a useful tool for the prediction of the optical/mechanical properties of the material as a result of the irradiation.

Η αλληλεπίδραση παλμών λέιζερ με μια ευρεία γκάμα στερεών (όπως μέταλλα, ημιαγωγοί, διηλεκτρικά, πολυμερή) δύναται να προκαλέσει σημαντικές τροποποιήσεις στην επιφάνεια αυτών και κατά συνέπεια αξιοσημείωτες μεταβολές στις οπτικές και μηχανικές τους ιδιότητες. Ένας ιδιαίτερα ξεχωριστός τύπος αλληλεπίδρασης λέιζερ-ύλης που επιτρέπει την έρευνα των υφιστάμενων μηχανισμών σε πολύ μικρή χρονική κλίμακα συνίσταται στη χρήση λέιζερ υπερβραχέων παλμών (της τάξεως των femtoseconds (fs). Η αλληλεπίδραση υλικών με τέτοιου τύπου παλμικά λέιζερ προκαλεί μία ποικιλία εξαρτώμενων διεργασιών σε χωροχρονικό επίπεδο που καθορίζεται από τα χαρακτηριστικά της ακτινοβόλησης. Στην εργασία αυτή, οι φυσικοί μηχανισμοί που περιγράφουν την απόκριση του υλικού μετά την ακτινοβόληση θα μελετηθούν με την επίλυση ενός συστήματος παραβολικών διαφορικών εξισώσεων με υπολογιστικές τεχνικές βασισμένες στη μέθοδο των πεπερασμένων διαφορών. Η τεχνική αυτή θα επιτρέψει την διεξοδική μελέτη των θερμικών φαινομένων που εμφανίζονται τόσο στο ηλεκτρονικό σύστημα όσο και στο πλέγμα του υλικού και θα αποτελέσει παράλληλα ένα χρήσιμο εργαλείο για την πρόβλεψη των οπτικών/μηχανικών ιδιοτήτων του υλικού ως αποτέλεσμα της ακτινοβόλησης.

Acknowledgements

First of all I would like to thank my supervisor, Dr. Emmanuel Stratakis who gave me the opportunity to work with his group. Our collaboration made me interact with new aspects of science and especially the area of materials.
I am extremely grateful to my advisor Dr. George Tsibidis, for his guidance. I have had the pleasure of being in contact with him on a very regular basis and he has always taken the time needed to discuss problems regarding my project.
I owe great thanks to professors George N. Makrakis and Nikolaos K. Efremidis for their guidance and their consultation during my undergraduate career.

Antonios-Stylianos Valavanis

Contents

Bibliography **32**

List of Figures

List of Symbols

TTM	Two Temperature Model
fs	Femptosecond
ps	Picosecond
ns	Nanosecond
PDE	Partial Differential Equation
ODE	Ordinary Differential Equation
α	Optical Penetration Depth
$\vec{q}$	Heat flux density
S	Source Term
t_p	Pulse Duration
R	Reflectivity
E_p	Laser fluence
γ	Electron constant of specific heat
G	Electron-lattice coupling parameter
C_e	Electron heat capacity
C_l	Lattice heat capacity
k_e	Electron thermal conductivity
k_l	Lattice thermal conductivity
MOD	Method Of Lines

IC	Initial Conditions
BC	Boundary Conditions
TVD	Total Variation Diminishing
WENO	Weighted Essentially Nonoscillatory
α	Optical Penetration Depth
MD	Molecular Dynamics
FD	Finite Difference
FWHM	Full Width at Half Maximum
RHS	Right Hand Side

Chapter 1

Introduction

Researchers have been studying how lasers damage different materials for several decades. This has contributed both to the basic scientific understanding of highly nonequilibrium processes and to the promotion of various industrial applications. Over the years material processing with intensive laser radiation has found numerous applications such as micro–machining [15] and nano–technology [16]. What is more, laser techniques are also encountered in the medical world for the removal of biological tissues.

Selecting the most appropriate laser source is of a profound importance since it can affect the material processing result. It seems that for each process and material a most suitable laser source can be found. However, femtosecond (fs) pulse lasers are easily tailored to desired specifications and are more powerful and versatile tools compared to the nanosecond (ns) pulse lasers [17]. In addition, femptosecond (fs) pulses have been shown to be more advantageous concerning the microstructuring as they simultaneously result in sharper hole geometries and smaller damage extention. This can be attributed to the limited heat transfer perpendicular to the incoming laser pulse, which means that a smaller area around the laser spot is being affected.

Additional studies, both theoretical [1] and experimental [16], have been conducted for the purpose of investigating the processes taking place in the bulk material or the surface during or after the laser pulse. Due to the complex character of the processes involved at different time and length scales, theoretical and computational investigations are a challenging task. An important parameter to investigate, is the electron–lattice relaxation time which is representative for every material. When pulses become shorter than this time, the electrons and the lattice are out of thermal equilibrium and have to be described separately.

One theoretical approach that has been widely used to allow a detailed investigation of the process / mechanisms that characterise laser - matter interaction is the Two–Temperature Model (TTM). This model constitutes the basis of the simulations presented in this work. The TTM basically describes the lattice and the electron temperature evolution via two coupled inhomogeneous partial differential equations.

The structure of this thesis is organized as follow. In the first part, an introduction to the theoretical background is given in order to define the basic principles that occur during the irradiation of a metal sample. This process is described qualitatively and a model for ultra–short laser pulses in metals is presented along with the numerical methods that were used for approaching this process. Afterwards the implementation scheme of the basic equations is proposed, while in the last part, the results from the simulations of various scenarios are discussed.

Chapter 2

Theoretical Background

Before explaining the numerical methods that approach this kind of problems, it is very important to understand the mechanisms when an ultrashort laser pulse hits a metal. In the following chapter, important basic theories are defined.

2.1 Laser Pulses

Laser ablation is considered to be one of the most important techniques for material processing and is commonly used for mass removal. More specifically, it can drill extremely small holes through very hard materials such as metals.

The pulsed laser refers to a short time (e.g., milliseconds to femtoseconds) output. The irradiation of a solid surface by a long-pulsed (e.g., nanoseconds pulsed) laser beam, results in the initiation of the material's temperature rise due to the absorbed laser energy. Then, the thermal motion of the particles is accelerated. Once the absorbed energy exceeds the sublimation energy, these particles evaporate or sublimate and eventually become vaporized particles.

Lasers with long wavelength are not suitable for metal ablation, as most of the laser energy is reflected by the metal surface. On the other hand, ultrashort laser pulses (e.g., femtosecond laser) allow even less thermal damage and a nearly melt free ablation, in case the laser pulses are close to ablation threshold. For this reason, ultrashort laser pulses are good candidates for metal ablation and constitute the kind of pulses that we are studying in this work. The differences between long (a) and short (b) laser pulses are shown in Figure 2.1.

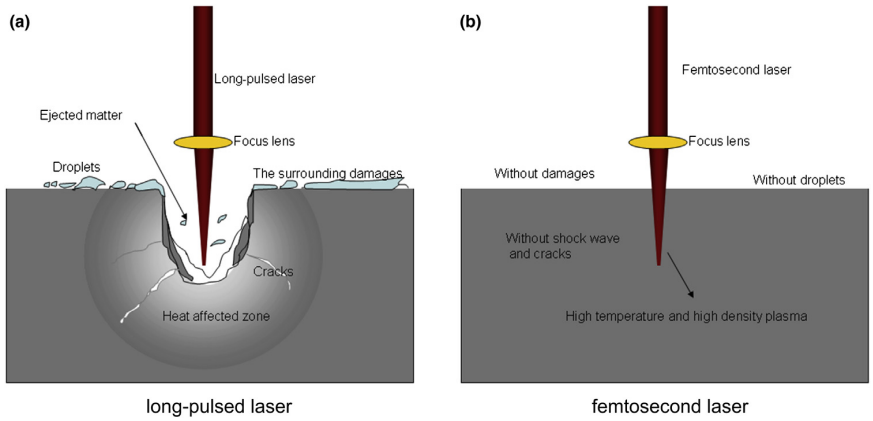

Figure 2.1 The characteristics of different laser ablation processes [21]

2.2 Thermal Diffusion

The key feature to short pulse damage is its distinct non-thermal behaviour resulting from the fact that the electron and lattice temperatures are far from equilibrium. However, that doesn't mean that there are no thermal processes involved at all. For short pulse damage the electrons and lattice are never in equilibrium during the laser pulse (figure 2.2).

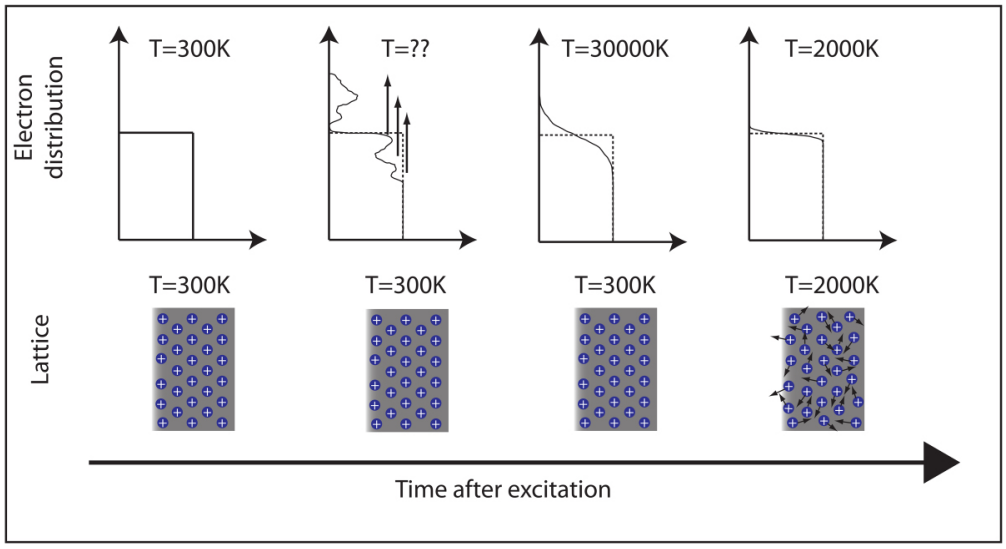

Figure 2.2 Sketch of the early excitation and relaxation processes in laser-irradiated metal. Initially, the electronic system is excited to a non-equilibrium distribution. Thermalisation to a new Fermi-Dirac distribution of elevated temperature is depicted before relaxation with the lattice to a joint temperature. [1]

Nevertheless, the lattice will always be in a thermal distribution. Quickly after the laser interaction the electrons will also form a thermal distribution within themselves via Coulomb collisions, but at higher values of temperature than the ions. So while it is not possible to treat the entire system as if it were in thermal equilibrium, the two components individually are in a thermal configuration and thus thermal effects are prevalent. Hence, it is possible to make sensibly accurate predictions for damage threshold fluences of materials using only thermal processes. As long as the electrons and lattice are handled separately, the expression for heat flow can still be expressed as:

$$\vec{q_{e,l}} = -k_{e,l}\nabla T_{e,l} \tag{1}$$

where $\vec{q}$ is the heat flux density, T is the local temperature, and k is the material conductivity, and where the subscripts e and l denote the electron population and the lattice population, respectively.

2.3 Ablation Model

Laser ablation or photoablation is the process of removing material from a solid surface by irradiating it with a laser beam. At low laser flux, the material is heated by the absorbed laser energy and evaporates or sublimates. At high laser flux, the material is typically converted to a plasma. Usually, laser ablation refers to removing material with a pulsed laser.

The physical image of femtosecond laser ablation is quite different from nanosecond laser ablation. When the pulse duration time is in the order of a femtosecond, the impact of the relaxation time of electron–phonon interaction should be considered. When the femtosecond laser focuses on the surface of a metal, the photon energy is first absorbed by electrons, leading to an accelerated thermal motion of the electrons and a rapid temperature increase of the electron subsystem. However, during the short pulse, there is no time for the electron's obtained energy to be transmitted to the lattice. At this point, the temperature of the electron gas is very high, while the lattice subsystem's temperature is maintained relatively low. Thus, a 'cold' ablation process occurs. Usually, the thermal equilibrium time of the metal is roughly a few femtoseconds. This is in fact the relaxation time of electron–phonon interaction.

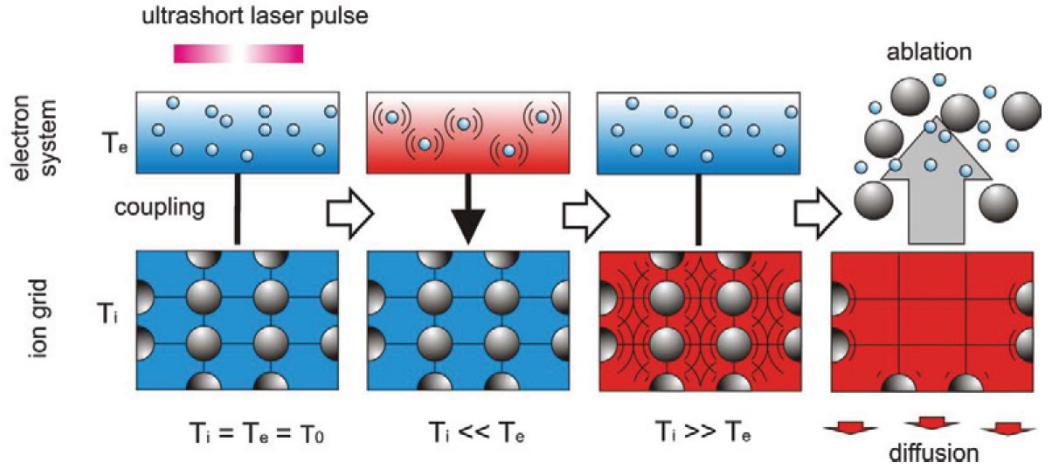

Figure 2.3 Processes of ablation in metals. After the pulse energy is absorbed, the electrons thermalize quickly, electrons transfer their energy to the lattice. Then, ablation and diffusion occurs [6]

In the short period of pulse, there are two temperature subsystems in the target: the electronic subsystem and the lattice subsystem. These two subsystems can be described using two electron–phonon coupling thermal conduction equations, named as the two-temperature model for femtosecond laser ablation.

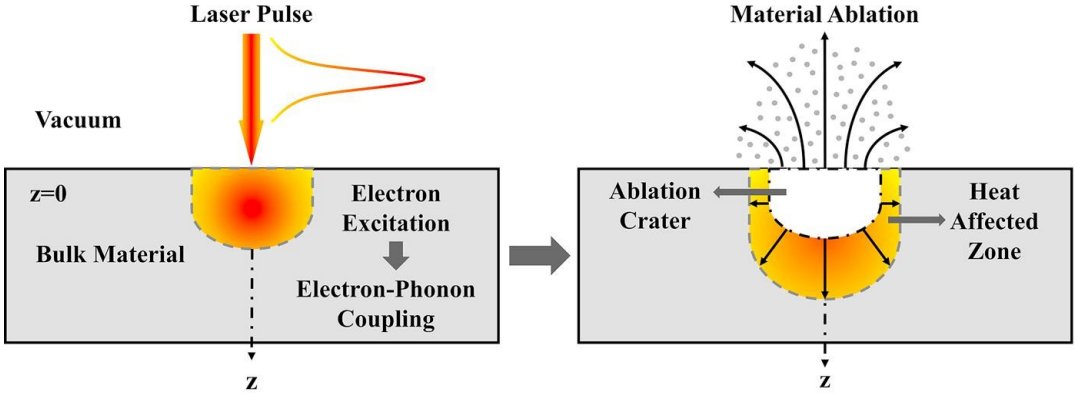

Figure 2.4 Ultrafast laser beam - metal interaction [2]

2.4 Modeling Laser Damage

2.4.1 Two-Temperature Model (TTM)

The theoretical method to examine the ultrashort laser-matter interaction is widely known as the Two-Temperature Model (TTM). Laser energy is absorbed in metals by the conduction band electrons within a few femtoseconds. After the fast thermalization of the laser energy in the conduction band electrons may quickly diffuse and thereby transport their energy deep into the lattice through electron-phonon coupling. The thermodynamic equilibrium between electrons and lattice is accomplished within tens to hundreds of picoseconds after the end of the pulse. Two differential equations, referred to as TTM [1], are combined to describe the temperature evolution of electrons and lattice, respectively

$$C_e \frac{\partial T_e}{\partial t} = \nabla \cdot (k_e \nabla T_e) - G(T_e - T_l) + S \tag{2}$$

$$C_l \frac{\partial T_l}{\partial t} = \nabla \cdot (k_l \nabla T_l) + G(T_e - T_l) \tag{3}$$

where the subscripts e and l refer to the electron and lattice parameters.
C_e and k_e are the heat capacity and thermal conductivity of electron, C_l is the lattice heat capacity which can be considered as a constant, the electron-phonon coupling G is dependent on the temperature. To capture the temperature dependency of material thermal properties we assume that C and k are also temperature depended variables.

Considering temporally Gaussian-shape pulsed laser irradiation, the time and space dependent source term can be expressed as

$$S(r,z,t) = I_0 exp\left(-4\ln(2)\frac{(t-t_0)^2}{t_p^2}\right)\frac{1}{\delta}(1-R)exp\left(\frac{-z}{z_0} - (\frac{r}{r_0})^2\right) \tag{4}$$

$$I_0 = \sqrt{\frac{4\ln(2)}{\pi}}\frac{E_p}{t_p} \tag{5}$$

Laser absorption from the surface into the bulk metal follows Lambert-Beers law [1], where R is the target reflection coefficient, δ is the optical penetration depth of the metal film. The laser pulse is a Gaussian distribution both in time and space, E_p is the laser fluence, r_0 and z_0 are the r-coordinate and z-coordinate radius of the laser spot and t_p is the Full Width at Half Maximum (FWHM) pulse duration. For t_0, we assume $t_0 = 3t_p$. The laser absorption into the work piece begins at r=z=0.

2.4.2 Boundary Conditions

In our latter simulations of laser ablation, finite-difference method is used to solve equations (1) and (2). The simulation starts at time t=0, and the initial conditions for both electrons and lattice are fixed at room temperature. As the ablation process takes place during the femtosecond to picosecond time period, it is reasonable to assume that heat losses from the metal film to the surrounding can be ignored. Therefore, the initial and boundary conditions can be described by

$$T_e(r, z, t = 0) = T_l(r, z, t = 0) = 300K \tag{6}$$

$$\left.\frac{\partial T_e}{\partial n}\right|_{\Omega} = \left.\frac{\partial T_l}{\partial n}\right|_{\Omega} = 0 \tag{7}$$

where Ω represents the four boundary surfaces of the 2D film

Chapter 3

Numerical Methods

Numerical methods aiming to depict the TTM and describe the transient dynamics of the electron gas - lattice subsystems. Through this representation, information such as Temperature evolution and melting can be noted. Consequently, detailed information about the dynamics of the system can be gathered. There are several numerical methods of solutions for these kind of problems. In this thesis Finite Difference method were used to approach the model.

3.1 Method of Lines

The basic idea of the Method Of Lines (MOL) is to replace the spatial derivatives in the Partial Differential Equation (PDE) with algebraic approximations. Once this is done, the spatial derivatives are no longer expressed explicitly in terms of the spatial independent variables. Thus, in effect only the initial value variable, typically time in a physical problem, remains. In other words, with only one remaining independent variable, we have a system of Ordinary Differential Equations (ODEs) that approximate the original PDE. The challenge, then, is to formulate the approximating system of ODEs. After this is done, we can apply any integration algorithm for initial value ODEs to compute an approximate numerical solution to the PDE. Thus, one of the prominent features of the MOL is the use of existing, and generally well established, numerical methods for ODEs.

As mentioned at the beginning of this chapter, the finite difference method is used for developing discrete nodebased approximations to derivatives.

3.1.1 Finite Difference

To illustrate this procedure, we consider the MOL solution of equations (2),(3). First we need to replace the spatial derivatives with an algebraic approximation. In this case we will use a finite difference (FD) such as

$$\left.\frac{\partial T}{\partial x}\right|_{x=x_o} \approx \frac{T(x_o+h)-T(x_o-h)}{2h} \tag{8}$$

where x_o is the grid point where the derivative is numerically calculated and h is the spacing along the x-axis assumed constant for the time being.

We should also mention two points of terminology for FD approximations. The equation (8) is a centered approximation since the two points at x_o+h and x_o-h are centered around the point x_o (Figure 3.1). However, there are also examples of noncentered, one-sided or upwind approximations since the points x_o and x_o-h are not centered with respect to h. Another possibility would be to use the points x_o and x_o+h in which case the approximation of T_x would be downwind. These are called backward and forward approximations accordingly.

The numerical error for the centered approximation is of the order of $\mathcal{O}(h^2)$ in addition with the forward or backward method which is of the order of $\mathcal{O}(h)$. For this reason, to obtain more accurate results, in the derivative approximations of this work, centered approximation is used.

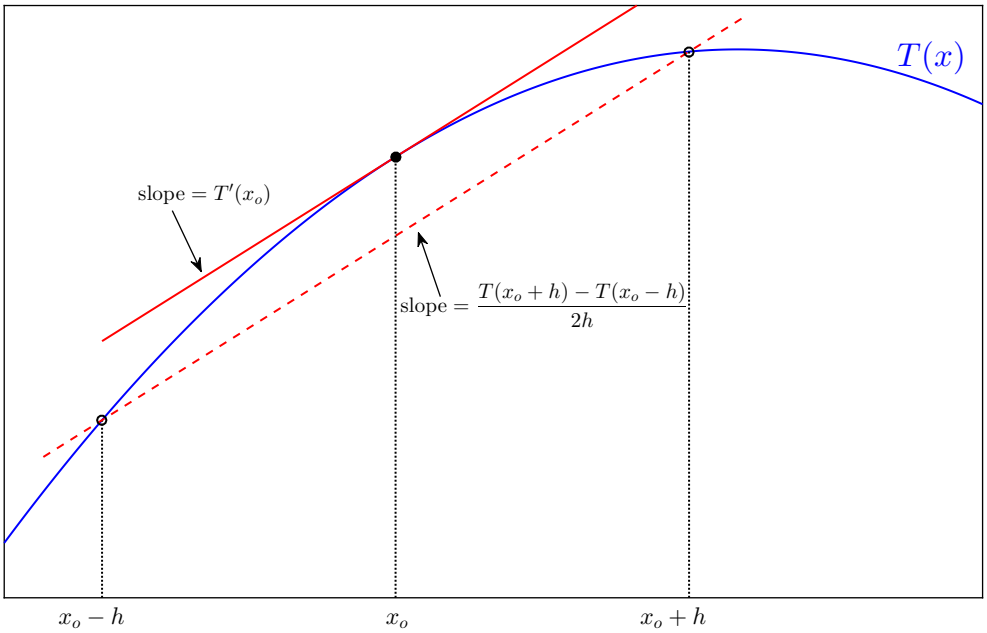

Figure 3.1 Centered Finite Difference method

Finally, to conclude the discussion of first order PDEs, since the Godunov theorem indicates that FD approximations above first order will produce numerical oscillations in the solution, the question remains if there are approximations above first order that are nonoscillatory. In order to answer this question we note that the Godunov theorem applies to linear approximations. Equation (8) is a linear approximation. If, however, we consider nonlinear approximations for T_x, we can in fact develop approximations that are nonoscillatory. The details of such nonlinear approximations are beyond the scope of this discussion, so we will merely mention that they are termed high resolution methods which seek a total variation diminishing (TVD) solution. Such methods, which include flux limiter [23] and weighted essentially nonoscillatory (WENO) [24] methods, seek

to avoid non-real oscillations when shocks or discontinuities occur in the solution.

So far we have considered only the MOL solution of first order parts. We also need an approximation for the second derivative T_{xx}. A commonly used second order, central approximation is

$$\left.\frac{\partial^2 T}{\partial x^2}\right|_{x=x_o} \approx \frac{T(x_o+h)-2T(x_0)+T(x_o-h)}{h^2} \tag{9}$$

The numerical error of this approximation is of the order of $\mathcal{O}(h^2)$.

3.1.2 Time Discretization

As noted in subsection 3.1.1, both forward and backward approximations have notable temporal truncation errors. On the other hand, there are unconditionally stable methods such as the Crank–Nicolson method. This makes it an attractive choice for computing unsteady problems since accuracy can be enhanced without loss of stability at almost the same computational cost per time step.

Nevertheless, the discretization of the problem is not alterable. For this reason, MOL combined with centered finite difference approaches for spacial derivatives are used in the present work. This kind of approaches, have been widely used in various studies similar with this [3,9,19]. Moreover, for the requirements of our project the method is well responding and hence we obtain reliable results that also corresponds to the experimental data.

Concerning the time discretization part of MOL, a wide range of numerical methods can be used. These include Euler method, Runge-Kutta methods, variable multistep methods etc. In the present work, we will use a build-in solver of MATLAB, in order to obtain more accurate results, using a dynamical changing timestep size.

In particular beginning at the initial time and with initial conditions, MATLAB ODE solvers step through the time interval, computing a solution at each time step. If the solution for a time step satisfies the solver's error tolerance criteria, it is a successful step. Otherwise, it is a failed attempt. Then, the solver shrinks the step size and tries again.

Usually, the system of ODEs obtained after space discretization is quite stiff. For a stiff problem, solutions can change on a time scale that is very short compared to the interval of integration, but the solution of interest changes on a much longer time scale. Methods not designed for stiff problems are ineffective on intervals where the solution changes slowly because they use time steps small enough to resolve the fastest possible change.

Stiff solvers can be used exactly like the other solvers. However, you can often significantly improve the efficiency of the stiff solvers by providing them with additional information about the problem. There are four solvers designed for stiff (or moderately stiff) problems:

• **ode23s** is based on a modified Rosenbrock formula of order 2.
• **ode23t** is an implementation of the trapezoidal rule using a "free" interpolant.
• **ode23tb** is an implicit Runge-Kutta formula with a first stage that is a trapezoidal rule step and a second stage that is a backward differentiation formula of order two.
• **ode15s** is a variable-order solver based on the Numerical Differentiation Formulas (NDFs). Optionally it uses the Backward Differentiation Formulas, BDFs, (also known as Gear's method) that are usually less efficient. Ode15s is a multistep solver.

In this thesis, ode15s is employed for time discritization due to the stiff character of the TTM problem.

3.2 Stability

A critical issue with any time advancement scheme is its underlying stability. The stability criterion may be written as

$$\alpha \frac{\Delta t}{\Delta x^2} \leq \frac{1}{2} \tag{10}$$

The quantity, $\alpha\,\Delta t/(\Delta x)^2$, is a nondimensional quantity and it is called grid Fourier number [25]. Furthermore, α denotes thermal diffusivity.

For fixed grid spacing, Δx, Eq. (10) is equivalent to placing a restriction on the time step that may be used to attain a stable solution with explicit time advancement:

$$\Delta t \leq \frac{1}{2}\frac{\Delta x^2}{\alpha} \tag{11}$$

One of the important implications of Eq. (11) is that the time step size must also be correspondingly adjusted to a smaller value if the grid is refined. This requirement places a severe burden on computational efficiency. For example, if the grid size is halved, the time step size must be reduced by a factor of 4. This implies that, even for a 1D problem, the computational time needed to reach a certain instant of real time will go up by a factor of 8 if the grid size is halved. Thus, even though the explicit time advancement method is advantageous from the point of view of memory and ease of implementation, it can become computationally quite expensive when used for fine grids because of the restriction on the time step size that can be used.

If such stability analysis were to be performed on a spatially 2D PDE, the following stability criterion would result for the explicit method:

$$\alpha\Delta t[\,\tfrac{1}{(\Delta x)^2}+\tfrac{1}{(\Delta y)^2}]\leq\tfrac{1}{2} \tag{12}$$

For equal grid spacing in the two Cartesian directions (i.e., $\Delta x = \Delta y$), Eq. (12) reduces to

$$\Delta t\leq\tfrac{1}{4}\tfrac{(\Delta x)^2}{\alpha} \tag{13}$$

which implies that the restriction on the time step is even more severe for multidimensional problems [25].

3.3 Different Coordinate Systems

In order to trace our problem to a simplified manner, geometrical properties are taken under consideration. In order to do that the symmetry of a metal sample is being exploited and thus we can simplify our model. Different coordinate systems analysis can in principle be carried out. For this reason, diffusion equation can be generalized to

$$\tfrac{\partial u}{\partial t}=\alpha\,\nabla^2 u \tag{14}$$

where ∇^2 is the coordinate independent Laplacian operator which can then be expressed in terms of a particular coordinate system. For example, in cylindrical coordinates Eq. (14) is

$$\tfrac{\partial u}{\partial t}=\alpha\left(\tfrac{\partial^2 u}{\partial t^2}+\tfrac{1}{r}\tfrac{\partial u}{\partial r}+\tfrac{1}{r^2}\tfrac{\partial^2 u}{\partial\theta^2}+\tfrac{\partial^2 u}{\partial z^2}\right) \tag{15}$$

There is also an expression with shperical coordinates

$$\tfrac{\partial u}{\partial t}=\alpha[\,\tfrac{\partial^2 u}{\partial r^2}+\tfrac{2}{r}\tfrac{\partial u}{\partial r}+\tfrac{1}{r^2}\left(\tfrac{\partial^2 u}{\partial\theta^2}+\tfrac{cos\theta}{\sin\theta}\tfrac{\partial u}{\partial\theta}\right)+\tfrac{1}{r^2 sin^2\theta}\tfrac{\partial^2 u}{\partial\phi^2}] \tag{16}$$

The challenge then in applying the MOL to PDEs such as equations (15) and (16) is the algebraic approximation of the Right Hand Side (RHS) ($\nabla^2 u$) using FDs approximations, that have been used in MOL analysis. A particularly demanding step is regularization of singularities such as at r = 0 (note the number of divisions by r in the RHS of equations (15) and (16)) and at $\theta = 0$, $\pi/2$ (note the divisions by $sin(\theta)$ in Eq. (16)).

The complexity of the numerical solution of higher dimensional PDEs in various coordinate systems prompts the question of why a particular coordinate system would be selected over others. The mathematical answer is that the prudent choice of a coordinate system facilitates the implementation of the BCs in the numerical solution.

The answer based on physical considerations is that the coordinate system is selected to reflect the geometry of the problem system. For example, if the physical system has the shape of a cylinder, cylindrical coordinates would be employed. This choice then facilitates the implementation of the BC at the exterior surface of the physical system (exterior surface of the cylinder). However, this can also lead to complications such as the r = 0 singularities in Eq. (15) (due to the variable 1/r and $1/r^2$ coefficients). The resolution of these complications is generally worth the effort rather than the use of a coordinate system that does not naturally conform to the geometry of the physical system. Whether the physical system is not shaped in accordance with a particular coordinate system, i.e., has an irregular geometry, then an approximation to the physical geometry is used, generally termed body fitted coordinates.

In our 2D model, an approximation, cylindrical coordinates are used to discritize the metal sample and consequently solve the PDE system. However, as it is refered above, our model seems to be functional under specific circumstances. Therefore, axisymmetric properties of the sample needs to be taken into account.

3.3.1 Cylindrical Model

Inital and Boundary Conditions

The cylindrical domain is limited by the side surface and two bases. The surfaces $r = R_0$ (external radius of domain) and z = Z (bottom base of cylinder) are far enough away from the source resulting from the laser's action, that adiabatic conditions can be accepted both for R_0 and Z. A similar condition can be assumed for z = 0.

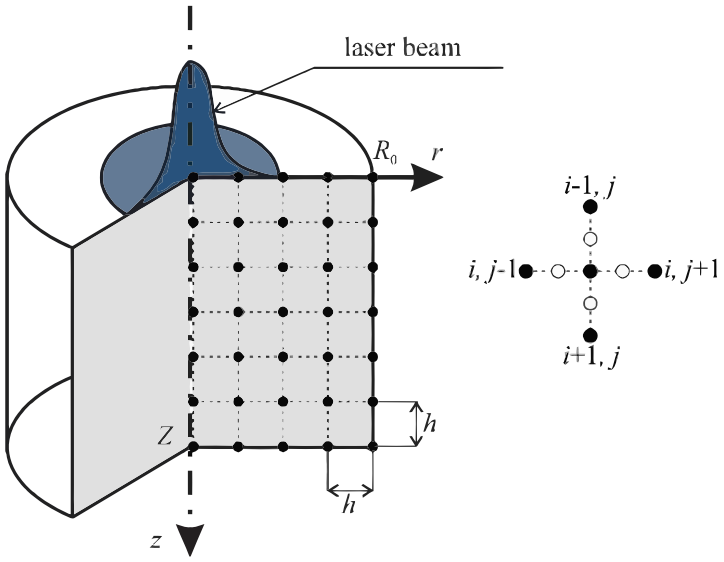

Figure 3.2 Differential mesh in Cylindrical Coordinates [14]

The Two-Temperature Model can be expressed as:

$$C_e \frac{\partial T_e}{\partial t} = \left(\frac{\partial^2 (k_e T_e)}{\partial r^2} + \frac{1}{r} \frac{\partial (k_e T_e)}{\partial r} + \frac{\partial^2 (k_e T_e)}{\partial z^2} \right) - G(T_e - T_l) + S \tag{17}$$

$$C_l \frac{\partial T_l}{\partial t} = \left(\frac{\partial^2 (k_l T_l)}{\partial r^2} + \frac{1}{r} \frac{\partial (k_l T_l)}{\partial r} + \frac{\partial^2 (k_l T_l)}{\partial z^2} \right) + G(T_e - T_l) \tag{18}$$

The numerical solution of Eq. (17), (18) depends upon the explicit finite difference technique to calculate the electron and lattice temperature distribution of plume through r and z axes. In the figure 3.1, the application of the centered approximation of Finite Difference method can be observed. Indices i and j will be used for indicating the points along the z and r directions respectively.

Chapter 4

Results & Discussion

The TTM given by the equations (2) and (3) can be readily solved numerically to analyse the heat penetration into the bulk of the material. We have set under investigation both the one dimensional model and the 2D model. Simulations are presented by choosing gold as a test material.

4.1 1D model

The parameters of our simulations are given in Table I, obtained from [8]. The electron heat capacity is calculated proportional to the electron temperature when the electron temperature is less than the Fermi temperature as $C_e = \gamma T_e$ [8]. The lattice heat capacity is set as a constant because of its relatively small variation as the temperature changes. The electron heat conductivity is expressed as $k_e = k_{e_0} B T_e/(A T_e^2 + B T_l)$ [8], where k_{e_0}, A and B are the material constants. For the electron–lattice coupling factor G we assume a temperature dependency $G = G_0(A(T_e+T_l)/B+1)$, where G_0 is the coupling factor at room temperature[8]. The lattice thermal conductivity k_l set as constant due to insignificant contribution. The penetration depth α is taken into account as $13.7\,nm$, obtained also from [8].

Table I. Thermophysical parameters of the system [8]

$G_0\,(10^{17} Jm^{-3}s^{-1}K^{-1})$	0.21
$\gamma\ (Jm^{-3}K^{-2})$	68
$A\ (10^7\, s^{-1}K^{-2})$	1.18
$B\ (10^{11}\, s^{-1}K^{-1})$	1.25
$k_{e_0}\ (Jm^{-1}s^{-1}K^{-1})$	318

4.1.1 Temperature evolution

The numerical method is first performed to calculate a 100nm thick single-layer gold film. The laser light source used in the simulation process is an 800 nm 100 fs laser with the laser fluence of 35 mJ/cm^2 and a pulse duration of the magnitude of $t_p = 100fs$. The surface reflectivity of gold is taken into account as a constant value R = 0.974. However, it would be important to mention that reflectivity coefficient constitute a variable value, depended on the characteristic time of laser pulse t_p [9].

The temperature evolution as a function of time, of the gold sample is shown in figure 4.1. Within the pulse interaction, the electron temperature is heated up to over a thousand K, while the lattice temperature remains low being close to the room temperature (300 K). It is noted that significant lattice heating occurs with the beginning of the relaxation, due to electron-phonon coupling, reducing the electron temperature simultaneously.

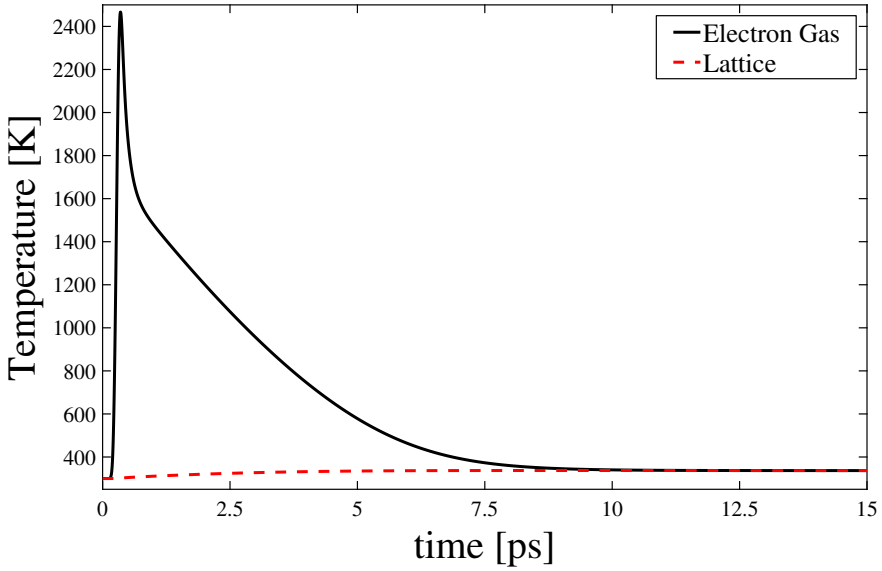

Figure 4.1 Electron T_e and lattice T_l temperatures versus time ($t_p = 100fs$, $E_p = 35mJ/cm^2$, 800 nm laser wavelength, $r = 0$)

The lattice temperature subsystem not much increase in compared with the electron subsystem. Briefly the behaviour of electron and lattice can be expressed as the electron temperature will be increased rapidly until the end of laser pulse, then decreased rapidly. Moreover for the lattice subsystem, the temperature profile increased slowly form the beginning of laser pulse and remain increased after the end of pulse duration (for several pulse duration times), due to large heat capacity for the lattice subsystem.

The thermal equilibrium between electrons and lattice is achieved afterward (the small plateau on the temperature curves). The time span between the initiation of ablation and the thermal equilibrium between electron and lattice is denoted as the ablation period, which depends on the electron-phonon coupling strength as well. It can be noted that once ablation starts, the decreasing rate of electron surface temperature is higher than the normal relaxation process

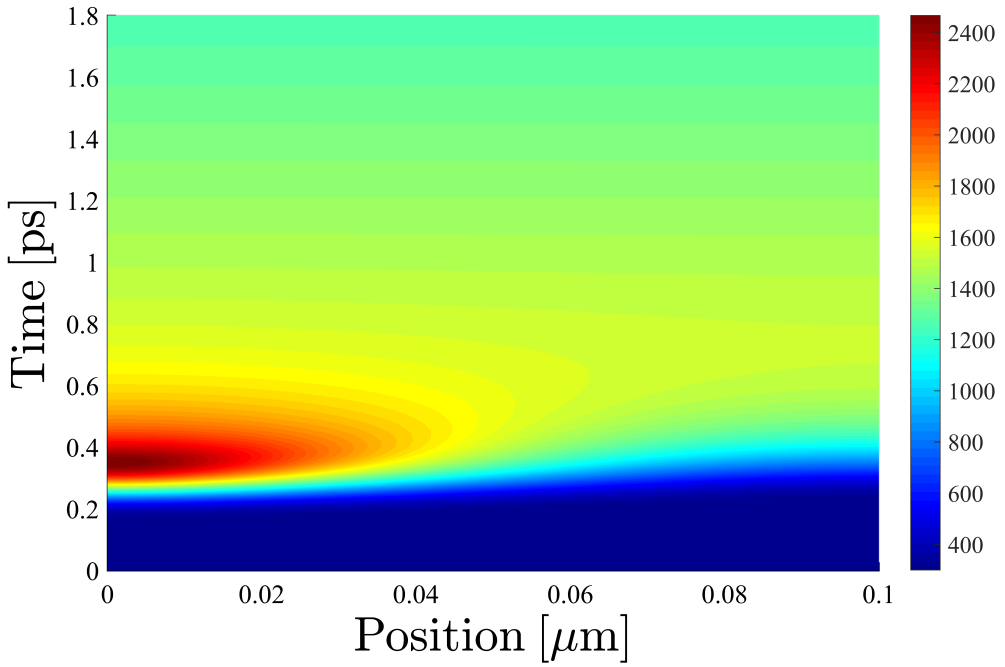

Figure 4.2 Electron temperature distribution versus time at $r = 0$ ($t_p = 100fs$, $E_p = 35mJ/cm^2$, 800 nm laser wavelength)

A contour plot for the electron temperature is shown in figure 4.2. This figure, vertical cuts, illustrates that the lattice remains cold for the first few picoseconds, and lattice then heated via electron–phonon collisions over a time-scale of a few picoseconds.

4.2 2D model

Both the physical and the optical parameters of the simulation are given in Table II. Various thermophysical parameters of the material, such as heat conductivities of the electron and lattice subsystems, calculated again in the basis of [8] and their calculation explained in the framework of the 1D model. The lattice heat capacity is set again as a constant. The electron heat conductivity is expressed as $k_e = k_{e_0} BT_e/(AT_e^2 + BT_l)$, with k_{e_0}, A and B represent material constants. As in the one-dimensional model, lattice thermal conductivity k_l set as constant. The penetration depth α is taken into account as $13.7\,nm$, obtained also from [8].

Table II. Thermophysical and optical physical parameters for the sample.[8,5]

$C_e\,(10^5 Jm^{-3}K^{-1})$	$fitting$
$C_l\,(10^6 Jm^{-3}K^{-1})$	2.5
$G\,(10^{17} Jm^{-3}s^{-1}K^{-1})$	$fitting$
$A\ (10^7\,s^{-1}K^{-2})$	1.18
$B\ (10^{11}\,s^{-1}K^{-1})$	1.25
$\alpha\ (10^{-9}m)$	13.7

As it can be noted from [5], electron heat capacity can be expressed with linear approximations, only in the limit of small Temperatures. Also, electron-phonon coupling factor should not be considered as constant in high temperature regime. For this reason, we calculate these parameters by using a fitting procedure with polynomial interpolation, in order to make our model more accurate. MATLAB functions that perform different forms of piecewise cubic Hermite interpolation were used. Each function differs in how it computes the slopes of the interpolant, leading to different behaviours when the underlying data has flat areas or undulations.

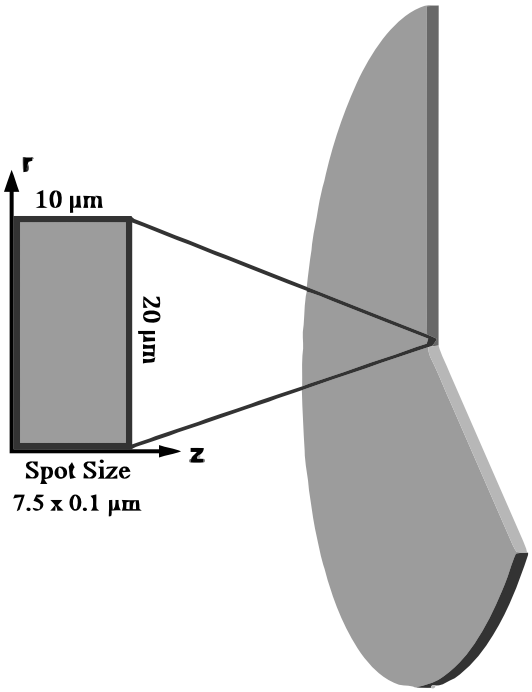

Figure 4.3 Geometric shape of the 2D metal sample (Modified from [4])

The numerical method is first performed to calculate a $r = 20\mu m \times z = 10\mu m$ gold sample (Figure 4.3). The laser light source used in the simulation process is an 500 fs laser with the laser fluence of 150 mJ/cm^2. The surface reflectivity of gold is taken again into account as a constant value R = 0.974.

Figure 4.4 represents the first half of the evolution of the laser pulse. We capture 4 frames until the Temperature reach a peak. It can be observed that a steep shift in the Temperature occurs in the z-axis. For that reason, in order to obtain more accurate calculations, we amplify the z-axis discritization with sufficient number of elements.

On the other hand, the slope of the diffusion in the r direction has a smooth behaviour. To avoid angularity into the plot, we choose appropriate spot size for the source term. A spot size of 7.5 x 0.1 μm (Figure 4.3) seems to be a good candidate for our simulations.

During the second half of the evolution, the same behaviour of the plot can be observed but in the opposite directions. The electron and the lattice subsystems tend to reach the thermal equilibrium after a couple of picoseconds.

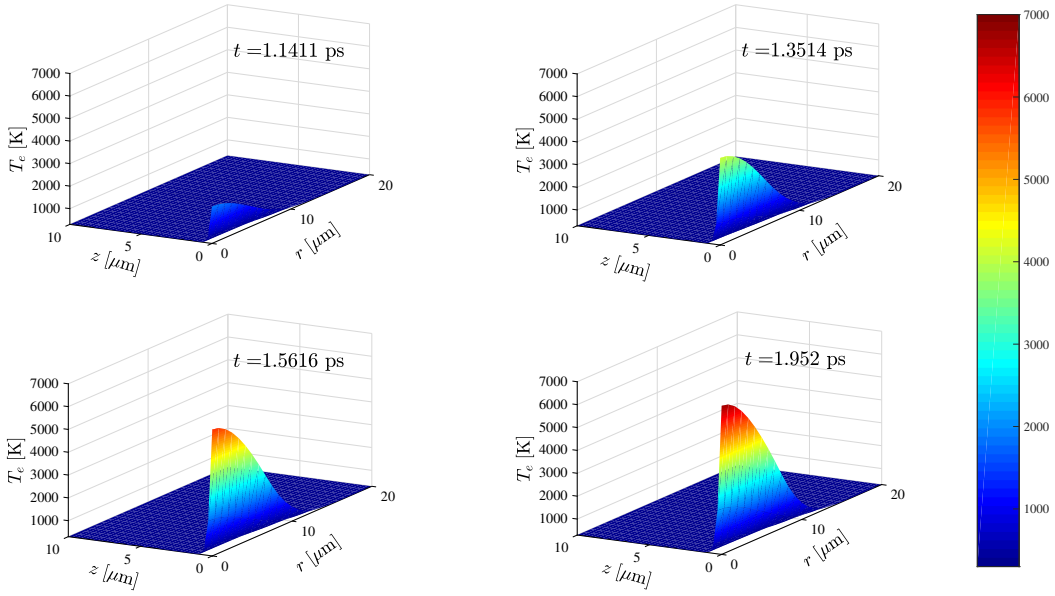

Figure 4.4 Distribution of electron temperature at four different frames of the evolution (t_p = 500fs, 800 nm laser wavelength, E_p=150 mJ/cm^2, r_0=7.5 μm, z_0=0.1μm)

The theoretical model presented Equations (2), (3) is suffice to describe the thermal response of the electron and lattice subsystems. The influence of various laser beam parameters such as the laser fluence E_p and the pulse duration t_p needs to be analysed in more details.

4.2.1 Fluence dependence

The role of various absorbed fluences in electron and lattice temperature is shown in Figure 4.5. It can be easily observed that fluence increasement, leads to higher peaks in the electron temperature. Also, it can be noted that the thermal equilibrium between electron and lattice is established after a few picoseconds for low fluences. At higher fluences, an approximate electron–lattice equilibrium is observed after more of picoseconds, and the energy is distributed over hundreds of nanometers due to heat propagation effects.

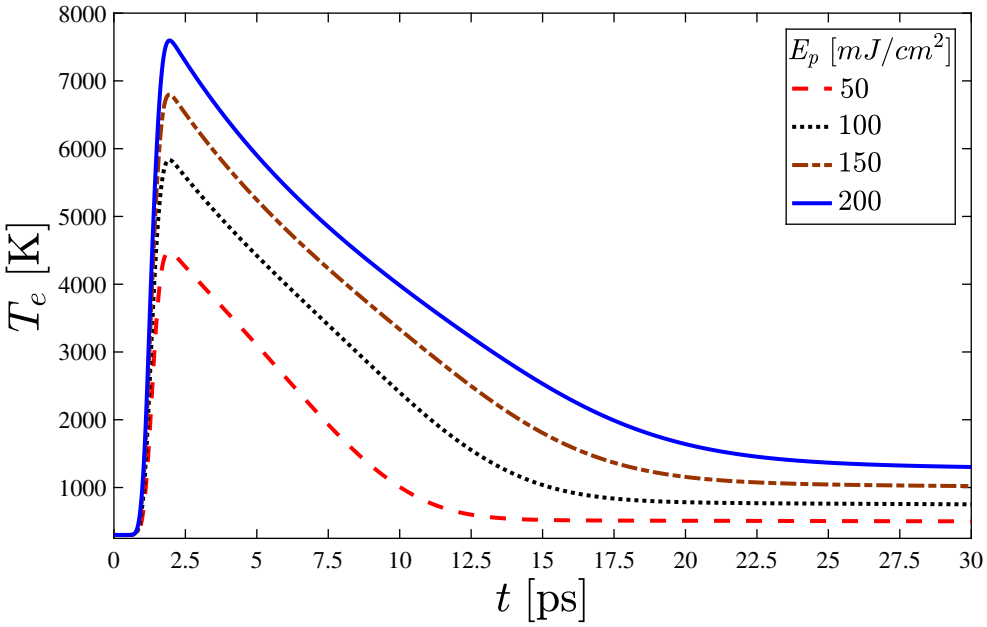

Figure 4.5 Transient behaviour of electron temperature, T_e for different expressions of laser fluence E_p (800 nm laser wavelength, $t_p = 500fs$ at $r = z = 0$).

It is important to mention that both widening and deepening of the craters appear for increasing laser fluences, while the depth of the ablation craters increases more quickly [3]. Under high fluence laser irradiation, both electron and lattice temperature rise faster to trigger a much earlier ablation.

This can be also noted from the lattice Temperature plot in Figure 4.6. Notable variations in the lattice temperature can be observed for different values of laser fluence. Consequently, upward trends in the fluence, enable the solid to reach the melting threshold value.

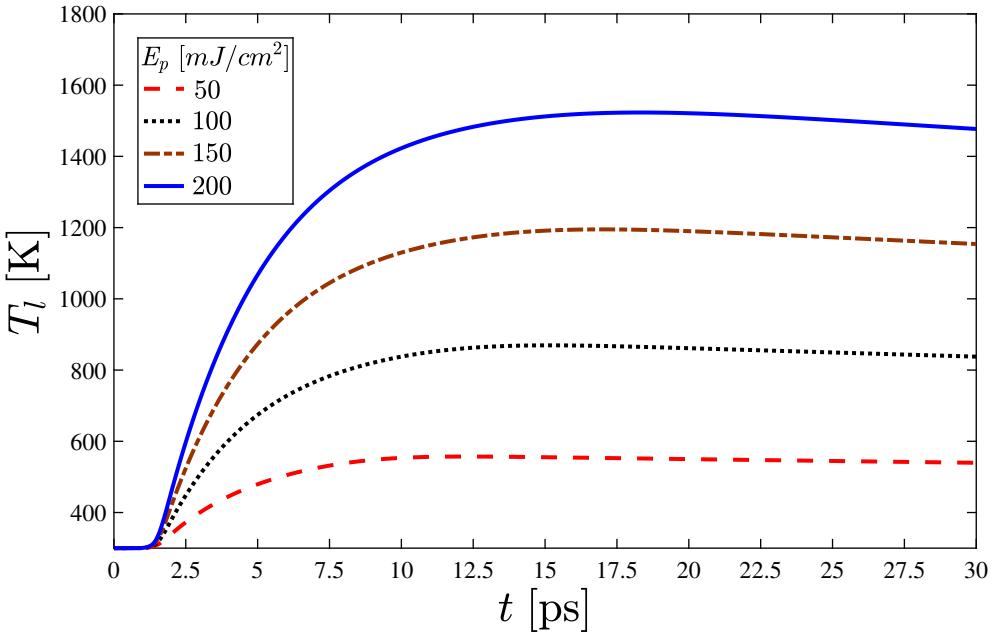

Figure 4.6 Transient behaviour of lattice temperature, T_l for different expressions of laser fluence E_p (800 nm laser wavelength, $t_p = 500fs$ at $r = z = 0$).

4.2.2 Pulse duration dependence

It is very important to investigate the effect of pulse duration on threshold fluence, which is related to electron and lattice temperatures.

After a couple of runs, for different laser pulse widths, we can notice that figure 4.7 show variations in peak electron temperature for different pulse durations. It is useful to note that the equilibrium temperature between electrons for longer pulse durations moves to higher times. Furthermore, temperature peak is decreased and moves to higher time values. In fact, the pulse duration in ultrashort regime is shorter than the electron-lattice coupling time.

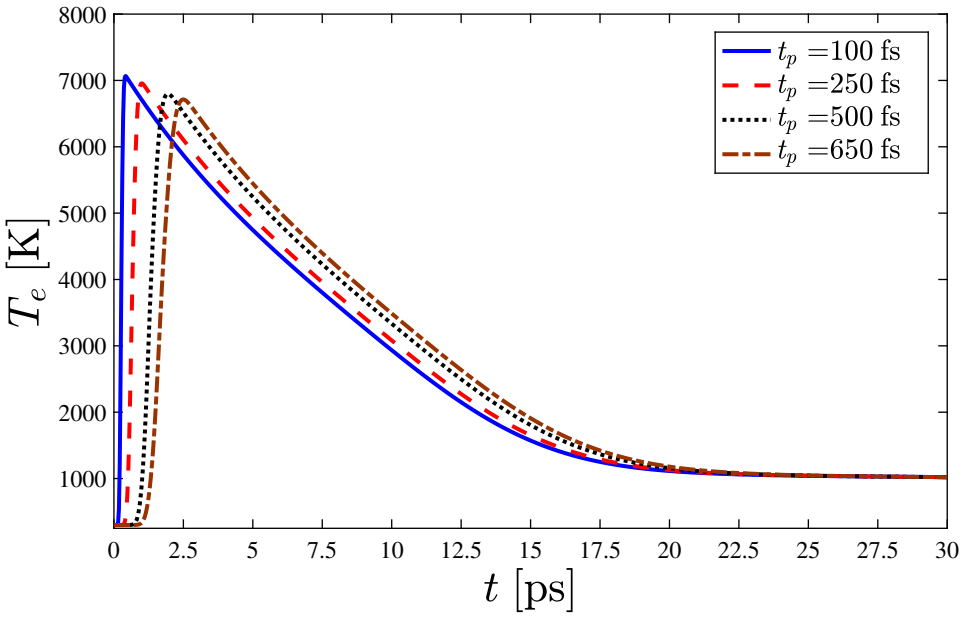

Figure 4.7 Electron temperature for different laser pulse widths (800 nm laser wavelength, $E_p = 150mJ/cm^2$, $r = z = 0$)

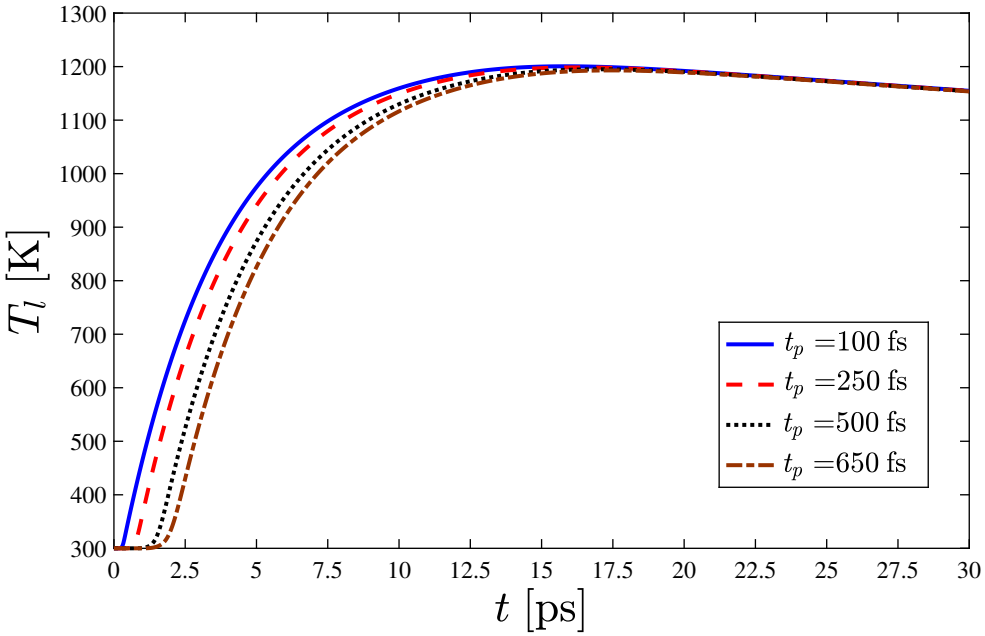

Figure 4.8 Lattice temperature for different laser pulse widths (800 nm laser wavelength, $E_p = 150mJ/cm^2$, $r = z = 0$)

The results, in Figure 4.8, show insignificant variations in peak lattice temperature for different pulse durations to reach the melting temperature of gold. Thus, the pulse duration in ultrashort regime does not play a major role in modifying the melting threshold value.

In comparison with Figure 4.7, with an increase in pulse width, the peak of electron temperature is decreased and moves to higher time values.

Chapter 5

Concluding Remarks & Future tasks

5.0.1 Concluding Remarks

The goal of this project is to present a detailed theoretical framework that describes the heat propagation through thin metal films. This need arose because recent pump-probe experiments failed to observe structural dynamics in different metal samples. Before the dynamics of the sample can be observed, the samples are irreversibly damaged by a high energy femtosecond laser pulse.

A theoretical background for the transient dynamics of the system during the laser interaction with thin metal samples is given. The two-temperature model describes the heating of the electrons and phonons in a lattice. The electron temperature will rise to high levels far above the lattice temperature before the electron-phonon coupling exchanges energy between the electrons and the lattice.

The two-temperature model with temperature-dependent optical and thermophysical properties were proposed to study thermal response for a gold sample irradiated by a femtosecond laser pulses. The system of the 2 time-dependent partial differential equations was developed in the cylindrical coordinates. Unlike the one-dimensional model, an axisymmetric model of finite geometry was employed to better understand the effects of multi-dimensionality on thermal wave generations.

In order to obtain significant informations of the system, versatile tools from the area of numerical analysis were used. A representation of the system in algebraic nodal equations were taken under consideration. This representation of the system constitutes the key point of the work. Derivative approximations by using Finite Difference method and adiabatic boundary condition in the surface were implemented.

The effect of the uncertainty in electron–phonon coupling constant and electron heat capacity were studied on two-temperature model output. A parametric analysis was performed for a range of pulse duration and fluence values with both reflectivity and the absorption coefficient are assumed to be static. In the numerical analysis, the laser pulse had a duration of 100 fs.

Finally, the following conclusions were drawn:

(1) Through the FD approximations, the model is not only able to describe the absorption of the laser energy by the electron gas, but also produce the fast diffusive heat transport which is characteristic for metals.

(2) Consideration of geometrical properties - symmetries of the irradiated sample and expression of the equations in a different coordinate system, can lead to more simplified calculations.

(3)Thermal response of the material is directly related to variations in pulse duration and fluence of the laser pulse.

5.0.2 Future Tasks

Although the presented methods are very promising, it seems that they are too simple for more complex systems. Also, it has to be noticed that only single pulse laser ablation into vacuum was studied. For typical applications like drilling, tens of thousands of pulses are needed.

Based on the current studies, several subjects are proposed for future work.

(1) First, it is very important to take under consideration the circumstances under which the damage of the material occurs. In particular, Navier-Stokes Equations can enrich our model, in order to obtain useful information when the liquid phase occurs. Also, including plastic deformations (e.g stresses, strains) can constitute noteworthy tools.

(2) Second, Quantum mechanical effects can broad our field of study and are needed to observe in microscale the exact behaviour of electrons during the interaction with ultrashort pulses (e.g electrons thermalisation).

(3) Third, dependence of the absorption coefficient from the various properties of the material (e.g the Black-body radiation) should be taken under consideration. Classical mechanics, represent invariable absorption coefficients which is unreliable, especially for metals in a short time regime.

(4) Last, it could be shown, that for suitable systems the combination of the Two–Temperature Model to molecular dynamics constitute a powerful tool to predict and describe what is happening in laser heated metals by ultra short pulses.

Bibliography

[1] Baerbel Rethfeld, Dmitriy S Ivanov, Martin E Garcia and Sergei I Anisimov, J. Phys. D: Appl. Phys. 50, 193001 (2017)

[2] Xiao Jia, Xin Zhao, Applied Surface Science 463, 781–790 (2019)

[3] Jinping Zhang, Yuping Chen, Mengning Hu, and Xianfeng Chen, Journal of Applied Physics 117, 063104 (2015)

[4] Qi, Xuele and Suh, C. Steve, Journal of Thermal Stresses, 32: 5, 477 - 493 (2009)

[5] Zhibin Lin, Leonid V. Zhigilei, and Vittorio Celli, Phys. Rev. B 77, 075133 (2008).

[6] J.P. Colombier, P. Combis, F. Bonneau, R. Le Harzic, E. Audouard, Phys. Rev. B 71, 165406 (2005)

[7] Karl-Heinz Leitz, B. Redlingshöfer, Y. Reg, A. Otto, M. Schmidt, Physics Procedia 12, 230–238 (2011)

[8] A.M. Chen, H.F. Xu, Y.F. Jiang, L.Z. Sui, D.J. Ding, H. Liu, M.X. Jin, Applied Surface Science 257, 1678–1683 (2010)

[9] George D Tsibidis, Journal of Applied Physics 123, 085903 (2018)

[10] Chen, J. K., & Beraun, J. E., Journal of Optics A: Pure and Applied Optics, 5(3), 168–173. (2003).

[11] M. Saghebfar, M. K. Tehrani, S. M. R. Darbani, A. E. Majd, Applied Physics A 123(1) (2016)

[12] J. K. Chen, J. E. Beraun, Numerical Heat Transfer Applications 40(1):1-20 (2001)

[13] George D. Tsibidis, E. Skoulas, and E. Stratakis, Optics Letters Vol. 40, Issue 22, pp. 5172-5175 (2015)

[14] Ewa Majchrzak, B. Mochnacki, Materials 11(11):2116 (2018)

[15] George D. Tsibidis, C. Fotakis, and E. Stratakis,
Physical Review B 92, 041405(R) (2015)

[16] Antonis Papadopoulos, E. Skoulas, A. Mimidis, G. Perrakis,G. Kenanakis, G. D. Tsibidis and E. Stratakis,
Advanced Materials, 1901123 (2019)

[17] B.N. Chicbkov, C. Momma, S. Nolte, F. von Alvensleben, A. Tünnermann,
Applied Physics A, Vol. 63, Issue 2, pp. 109-115 (1996).

[18] Antonis Papadopoulos, E. Skoulas, G. D. Tsibidis, E. Stratakis,
Applied Physics A 124:146, (2018)

[19] D.S. Ivanov, B. Rethfeld,
Applied Surface Science, Vol. 255, Issue 24, p. 9724-9728 (2009)

[20] J. K. Chen , W. P. Latham & J. E. Beraun,
Numerical Heat Transfer, vol. 42, issue 1, pp. 1-17 (2002)

[21] Saleem Hashmi editor in chief,
Comprehensive materials processing,Dublin City University

[22] M. Plexousakis, P. Chatzipantelidis,
Numerical Solution of Partial Differential Equations

[23] Wesseling P.
Principles of Computational Fluid Dynamics, Springer, Berlin (2001)

[24] Chi-Wang Shu,
Essentially Non-oscillatory and Weighted Essentially Non-oscillatory Schemes for Hyperbolic Conservation Laws, vol 1697. Springer, pp 325-432. 9, (1998)

[25] Sandip Mazumder,
Numerical Methods for Partial Differential Equations

[26] Adrienne S. Lavine, Frank P. Incropera, David P. DeWitt,
Fundamentals of heat and mass transfer

[27] Charles Kittel,
Introduction to Solid State Physics

[28] Neil W. Aschcroft, N. David Mermin,
Solid State Physics